Photoconductivity of Langmuir−Blodgett Monolayers of Silicon Nanoparticles

Sulolit Pradhan,[†] Shaowei Chen,*,[†] Jing Zou,[‡] and Susan M. Kauzlarich*,[‡]

Department of Chemistry and Biochemistry, University of California, Santa Cruz, California 95064, and Department of Chemistry, University of California, Davis, California 95616

The electronic conductivity of Langmuir−Blodgett monolayers of silane-passivated silicon nanoparticles (core diameter 3.86 ± 0.85 nm) was examined by electrochemical measurements within the context of photoirradiation and at controlled temperatures. Temperature dependence of the dark conductivity indicated that the interparticle charge transfer followed a thermal activation mechanism within the temperature range of 200−320 K; whereas at lower temperature, the ensemble conductance was determined by tunneling between (clusters of) nanoparticles that were of equivalent energy states. When exposed to photoexcitation with photon energy greater than the effective particle bandgap, the particle ensemble conductivity exhibited a drastic enhancement as compared to that in the dark; and, at a specific excitation wavelength, the conductivity became virtually independent of temperature. This suggested efficient ionization of the photoexcited quantum-confined electron−hole pairs by the applied electric field, most probably because of the relatively slow (radiative and nonradiative) recombination dynamics. Furthermore, whereas the photoconductivity increased with increasing photon energy in photoirradiation, the enhancement diminished gradually with increasing temperature, as a consequence of the combined effects of enhanced radiative and nonradiative recombination rate and increasing contribution from thermally activated interparticle charge transfer.

Introduction

Silicon nanoparticles have received a great deal of attention in recent years as a new functional material with unique physical/chemical properties that are unseen in the bulk form. For instance, whereas bulk silicon has been known to be poor light emitters because of the indirect bandgap characteristics, silicon nanostructures have exhibited interesting photo and electrochemical luminescent properties, and these properties are readily tunable simply by the nanoparticle dimensions and surface chemical functionalization due to the quantum confinement effects.[1−4] This unprecedented degree of control of the materials opto-electronic properties lays a solid foundation on which the silicon nanoparticles may be exploited as the effective building blocks for the fabrication of novel functional devices, such as single electron transistors, floating gate memories, biological and chemical sensors, as well as light-emitting devices.[5−8] These extensive research interests are also motivated by the ready integration into the current microelectronic industry where silicon is the mainstay material.[9,10] Within this context, a mechanistic understanding of the fundamental correlation between the particle structures and opto-electronic properties is a critical first step to realize the full technological potential.

A variety of physical and chemical approaches have been reported for the preparation of silicon nanoparticles, including ion implantation,[11,12] thermal vaporization,[13] laser ablation,[14,15] gas phase decomposition of silanes based on low-pressure nonthermal plasmon,[16] electrochemical etching by pulse anodization,[17] and electroreductive synthesis.[18,19] Notably, solution chemistry routes have also been reported which offer the striking advantages of ready manipulation of the particle dimensions

and surface chemical functionalization.[20−23] Of these, the silanization of methoxy-passivated silicon nanoparticles leads to the preparation of ultrastable luminescent nanoparticles,[21,24,25] in comparison to the alkoxy-terminated particles that have been made previously, rendering it possible to examine the optical and electronic properties in detail, and more significantly, to reversibly control the materials properties for durable utilization.

Similar to monolayer-protected transition-metal nanoparticles,[26−28] these silane-passivated silicon nanoparticles behave as nanoscale composite materials where the electronic conductivity properties are manipulated by both the semiconducting nanocrystalline core and the insulating organic layer. Importantly, like other semiconductor quantum dots (QDs), the photoactivity of the nanoparticle core may also be exploited as an additional powerful variable in the regulation of the ensemble conductivity.[4,13,29,30] For instance, in our previous studies of the photoconductivity of PbS and CdSe nanoparticle monolayers,[31,32] we observed a drastic enhancement of the particle conductivity when the monolayers were exposed to photoirradiation with the energy of the photons higher than the particle bandgap. However, these compound semiconductor nanoparticles are prone to decomposition, in particular, under photo and electrochemical excitation. Consequently, it has remained a challenge to reversibly control the photoconductivity of the particle ensembles.

By using the silane-passivated nanoparticles of elemental silicon, it is anticipated that the ensemble conductivity will be reversibly photoswitched because of the unique chemical stability. Bulk silicon exhibits an indirect bandgap of 1.1 eV (and a direct bandgap of 3.4 eV); whereas for nanometer-sized silicon nanoparticles, the gap can be enlarged substantially as a consequence of the quantum confinement effects, rendering it possible to use silicon nanoparticles for robust and reproducible UV to visible photodetection.[19] Thus, in this study, we will first employ the Langmuir−Blodgett (LB) method to fabricate

* To whom correspondence should be addressed. E-mail: schen@chemistry.ucsc.edu (S.W.C.); smkauzlarich@ucdavis.edu (S.M.K.).
† University of California, Santa Cruz.
‡ University of California, Davis.

Photoconductivity of LB Monolayers of Si Nanoparticles

J. Phys. Chem. C, Vol. 112, No. 34, 2008 **13293**

monolayers of silane-passivated silicon nanoparticles at selected interparticle separations, and then examine the electronic conductivity under photoirradiation of different wavelength and at controlled temperature. As demonstrated previously,[31,32] LB thin films of nanoparticle materials exhibit marked improvement of the long-range ordered arrangements of the nanoparticles as compared to solid films that are prepared by the dropcasting method. Thus, the ensemble conductivity can be better correlated to the nanoparticle structures and interparticle interactions. The interparticle charge transfer is anticipated to be accounted for by the interplay between charge hopping based on thermal activation and photoenhanced charge carrier concentrations.

Experimental Section

Chemicals. Silicon tetrachloride (99%, Acros), sodium naphthalide (98%, Acros), octyltrichlorosilane (98%, Acros), 1,2-dimethoxyethane (glyme, 99%, Acros), hexane (98%, Fischer), chloroform (98%, Acros), and methanol (98%, Fischer) were used as received. Water was supplied by a Barnstead Nanopure water system (18.3 MΩ).

Particle Synthesis. Octyltrichlorosilane (OTCS) capped silicon nanoparticles were synthesized according to the published method.[21,24,25] Briefly, chloride-terminated SiNP were first prepared by the reduction of silicon tetrachloride with sodium naphthalide. An excessive amount of methanol was then added, and the solution was under vigorous stirring for 12 h to afford methoxy terminated silicon nanoparticles. To this solution HPLC-grade H_2O was added in glyme followed by the addition of OTCS and heating first at 60 °C for 30 min and then at room temperature for 12 h. The resultant silanized particles were then collected in chloroform. The chloroform solution was purified by repeated extraction with a water/hexane mixture to yield a waxy, yellow-light solid which could be suspended in typical nonpolar organic solvents.

Spectroscopy. The particle core diameter was estimated by transmission electron microscopic (TEM) measurements. The samples were prepared by the evaporation of the colloids on a holey or continuous carbon-coated 400-mesh copper grid. The TEM micrographs were acquired with a Phillps CM-12 microscope operated at 120 kV and digitized by ImageJ for particle core size analysis. UV−visible spectroscopic measurements were carried out with a UNICAM ATI UV4 spectrometer, and the photoluminescence study was performed with a PTI Fluorescence Spectrometer. The typical concentration of the silicon nanoparticles solution was 0.1 mg/mL in chloroform and the same solution was used both in the UV−vis and fluorescence measurements. ^1H NMR spectra of the particle samples were acquired with a Varian Unity 500+ spectrometer at a particle concentration of 5 mg/mL in $CDCl_3$.

Langmuir−Blodgett Study. The monolayer films of these nanoparticles were prepared by the LB method at selected interparticle separations at room temperature. A known amount of the particle solution, typically at 0.45 mg/mL in chloroform, was first spread onto the water surface of a LB trough (NIMA 611D) by using a Hamilton microliter syringe, and at least 2 h were allowed for solvent evaporation before the first compression. The particle monolayer was then deposited at selected surface pressures onto an interdigitated array electrode (IDA, 25 pairs of gold fingers of 3 mm × 5 μm × 5 μm, from ABTECH) whose surface was coated a prior by a self-assembled monolayer of butanethiols to render it hydrophobic. The transfer ratio was close to unity suggesting a rather efficient deposition of the particles onto the electrode surface. Once deposited, the IDA electrode with the particle monolayer was washed with ethanol and dried gently with ultrahigh-purity nitrogen, before being transferred into a cryostat for electrochemical measurements.

Electrochemistry. Electrochemical measurements of the particle conductivity were then carried out in vacuum (Cryogenic Equipment, JANIS Research Co.) with an EG&G PARC 283 Potentiostat/Galvanostat. The sample temperature was controlled by a LAKESHORE 331 Temperature Controller within the range of 100−320 K. The photoconductivity was examined by shining four low-power lasers (CW mode, <25 mW, all from CrystaLasers) onto the nanoparticle monolayers through a quartz window: UV (355 nm), blue (473 nm), green (532 nm), and red (638 nm).

Results and Discussion

Figure 1 shows a representative TEM micrograph of the silane-passivated silicon nanoparticles. It can be seen that the particles are mostly of spherical shape and well dispersed with no apparent aggregation, suggesting that the particles are sufficiently protected by the silane monolayers. The inset depicts the core size histogram, where most of the particles can be found within a relatively narrow size range of 2−5 nm. From this, the average particle diameter is estimated to be 3.86 ± 0.85 nm, substantially smaller than the exciton Bohr radius of Si, 4.9 nm. Note that the blue shift of the optical absorption threshold of QD molecules can be correlated directly to the nanocrystal dimension (d)[33]

$$d \cong \sqrt{\frac{h^2}{2\Delta E_g}\left(\frac{1}{m_e} + \frac{1}{m_h}\right)} \tag{1}$$

where ΔE_g is the shift of QD bandgap energies relative to that of bulk materials, m_e and m_h are the effective electron and hole masses respectively ($m_e = 1.08m_0$ and $m_h = 0.56m_0$ for bulk silicon with m_0 being the electron rest mass[34]), and h is the Planck's constant. Thus, from eq 1, one can evaluate the effective particle bandgap based on the core dimension; and at $d = 3.86$ nm, $\Delta E_g = 0.27$ eV. As mentioned earlier, bulk silicon typically exhibit an indirect bandgap of 1.1 eV and a direct bandgap transition at 3.4 eV.[3,23] Nevertheless, the estimate of the nanoparticle bandgap based on eq 1 is smaller than that obtained from spectroscopic measurements detailed below.

Figure 2 depicts the excitation and emission spectra of the silicon particles in chloroform. It can be seen that there is a well-defined excitation peak at 300 nm, which corresponds to the excitonic absorption peak observed in the UV−vis spectroscopic measurements (inset), suggesting that the effective particle bandgap is about 4.14 eV. The disparity of this value from that estimated from eq 1 may be accounted for by the fact that in TEM measurements, all particles are taken into account in core size estimation whereas in fluorescence measurements, the major contributions are from the smaller particles (based on eq 1, the bandgap of 4.14 eV corresponds to a particle diameter of 2.33 nm). Similar behaviors were also observed previously with CdSe nanoparticles.[32]

Furthermore, when excited at 300 nm, a rather intense emission peak can be observed at 344 nm. This transition most likely arises from the electron−hole radiative recombination within the particle core which behave as direct bandgap materials; yet the slightly asymmetrical waveshape also implies additional (and less radiative) transitions involving surface trap states that occur at a somewhat longer wavelength position (and lower energy). Of note is that the emission peak position redshifts from 344 to 420 nm when the excitation wavelength moves from 290 to 370 nm (and at longer excitation wave-
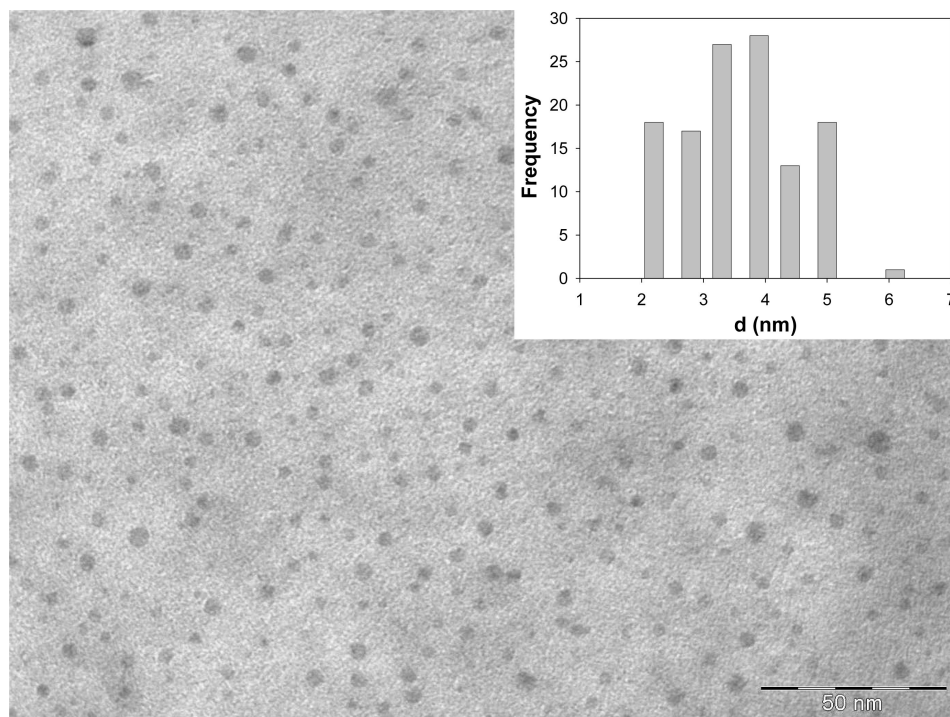
Figure 1. Representative TEM micrograph of silicon nanoparticles. Scale bar 50 nm. Inset depicts the corresponding core size histogram.
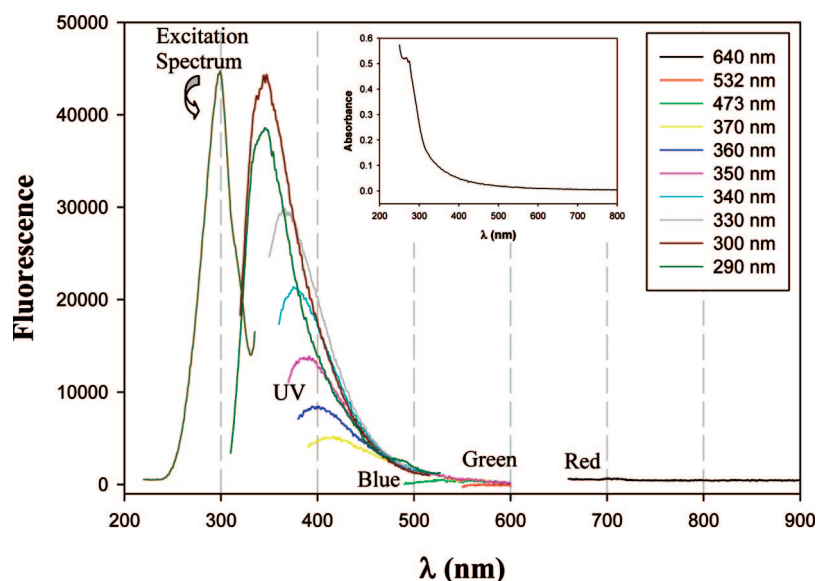

Figure 2. Fluorescence spectra of silicon nanoparticles in chloroform (0.1 mg/mL). The excitation spectrum was acquired with the emission wavelength (λ_{em}) set at 360 nm whereas the emission spectra were acquired at varied excitation wavelengths (λ_{ex}) as specified in figure legends. The photoluminescence profiles when excited by the four lasers (red, green, blue and UV) were also marked. Inset shows the UV−visible absorption spectrum of the same particle solution.

lengths, the emission becomes almost indistinguishable from the background); and the corresponding peak intensity also decreases. This may be attributable to at least two sources. The first is the core size dispersity of the silicon nanoparticles. That is, when excited at a longer wavelength, only the larger particles that have a smaller bandgap will contribute to the luminescence photons; whereas excitation at a shorter wavelength expands the contributions to smaller particles as well. From Figure 2, one can also see that indeed the predominant contribution to the photoluminescence is the smaller particles, as speculated above. The other explanation is based on particle surface trap states. With increasing excitation wavelength, the contributions from the core transitions diminish, and the radiative recombination from the surface trap states becomes increasingly dominant.

Considering the modest dispersity of the particle core size determined above, the observed photoluminescence properties are most likely the combined consequence of both factors.

The study of the nanoparticle photoconductivity was then carried out by using nanoparticle LB monolayers. Figure 3 shows a representative Langmuir isotherm of the silane-passivated silicon nanoparticles. The overall behaviors are very similar to those observed with other monolayer-protected nanoparticles.[31,32,35,36] First, the takeoff area (A_{TO}) can be identified to be ca. 135 cm^2. At surface areas much larger than A_{TO}, the particle monolayer exhibits a minimal surface pressure, corresponding to a two-dimensional gas phase; and upon mechanical compression, the surface pressure increases in a rather steep fashion, indicative of the formation of a condensed

Photoconductivity of LB Monolayers of Si Nanoparticles

J. Phys. Chem. C, Vol. 112, No. 34, 2008 **13295**
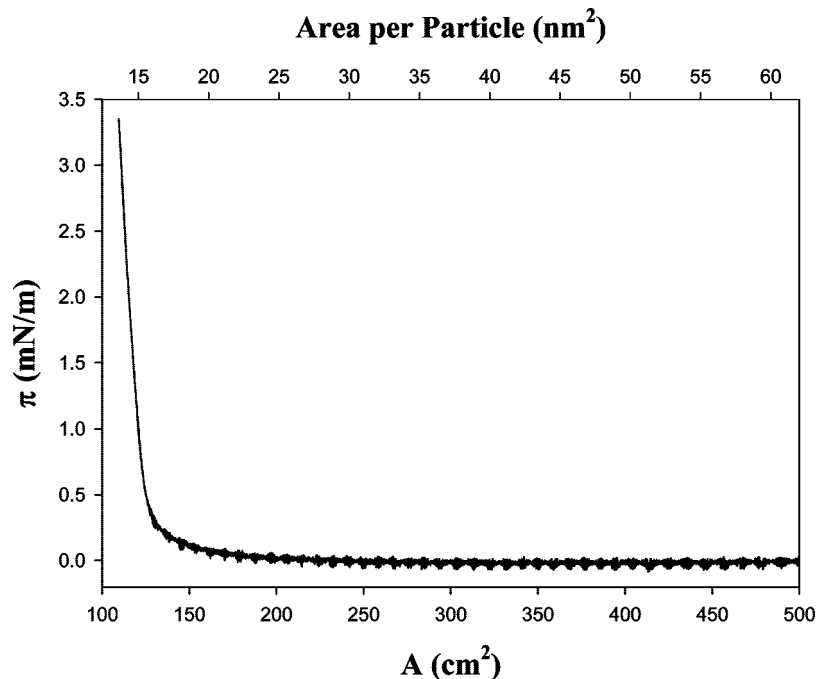
Figure 3. Representative Langmuir isotherm of the silicon nanoparticle monolayer at room temperature. Particle concentration 0.45 mg/mL in chloroform, amount sprayed 60 μL, and compression speed 10 cm^2/min. The takeoff area is 135 cm^2.

phase of the particle monolayer, most probably as a result of ligand intercalation between adjacent particles. A monolayer of particles was then deposited at a surface area of 109 cm^2 onto an IDA electrode surface by the LB technique (corresponding to an area of ca. 13.5 nm^2 per particle). This is smaller than the physical cross section of a particle, 30.4 nm^2, suggesting a packed structure of the particle monolayer (with ligand intercalation). The electronic conductivity was then evaluated by electrochemical measurements in vacuum and at different temperatures.

Figure 4A depicts the current–potential (I–V) profiles of the nanoparticle monolayers measured in the dark within the temperature range of 100–320 K. First, it can be seen that although the applied voltage bias is only ±1 V (corresponding to a DC electric field of up to 2 × 10^3 V/cm across the IDA fingers), which is substantially smaller than the spectroscopic bandgap of the particle core (Figure 2), appreciable currents (up to nA) can still be detected. This may be ascribed to the interparticle charge transfer that is facilitated by the particle surface defects,[32] as charge separation of surface trapped carriers occurs at lower energy than separation of carriers confined to the nanoparticle cores.[37] Second, the ensemble conductance increases rather markedly with increasing temperature, consistent with the semiconducting nature of the nanoparticle materials. In fact, from the slope of the I–V curves, the electronic conductivity of the nanoparticle monolayers can be estimated, as shown in Figure 4B, which exhibits an increase of 3 orders of magnitude when the temperature increases from 100 to 320 K. From Figure 4B, it can also be seen that at relatively high temperatures (200–320 K), the particle conductivity exhibits Arrhenius-type temperature dependence with an activation energy of 34.2 KJ/mol, implying a thermal activation mechanism for interparticle charge transfer, likely as a result of thermal population of the particle surface defect states.

In contrast, at low temperatures (<200K), the particle conductivity remains virtually invariant, where the interparticle charge transfer probably arises from electron tunneling between (clusters of) nanoparticles that are of equivalent energetic states

but not necessarily adjacent to each other, i.e., via the so-called variable-range hopping mechanism.[38] Such a temperature-dependent variation of charge transfer mechanisms has also been observed with ensembles of transition-metal nanoparticles[39,40] as well as semiconductor quantum dots.[38]

Furthermore, it should be noted that at room temperature the particle conductivity reaches ca. 0.1 mS/m, only about 1 order of magnitude smaller than that of bulk silicon (1.56 mS/m),[41] despite the long octylsilane protecting shell. Again, this is most probably because of the surface defect sites that serve as the charge transfer pathways between neighboring particles. Note that charge transfer between surface trap states has been proposed to account for the electrogenerated chemiluminescence of silicon nanoparticles in solution.[3] In nanoparticle solid ensembles, this charge transfer process will be further facilitated by the applied electric field.

The effect of photoirradiation on the conductivity of the nanoparticle films was then examined. Figure 5 shows some representative I–V profiles of the same particle monolayers with and without laser photoirradiation at two different temperatures: (A) 130 K and (B) 310 K. Note that the dark profiles are the same as those depicted in Figure 4. It can be seen that at 130 K, excitation by the red laser (638 nm) saw virtually no difference of the particle conductance as compared to the dark profile, whereas upon photoirradiation by the green (532 nm), blue (473 nm) and UV (355 nm) lasers, the current increased significantly. For instance, the particle conductivity is merely 1.5 × 10^{-4} mS/m in the dark or with the red laser; yet it increases by more than 3 orders of magnitude to 0.085, 0.13, and 0.18 mS/m, respectively, when excited by the green, blue, and UV lasers. At 310 K, a similar enhancement trend was observed of the particle photoconductivity with the four different lasers. However, the particle conductivity only saw a 2-fold increase upon photoexcitation, 0.075 mS/cm (dark), 0.076 mS/m (red), 0.081 mS/m (green), 0.13 mS/m (blue), and 0.19 mS/m (UV).

Panel (C) summarizes the variation of the nanoparticle conductivity at different temperatures in the dark and in the
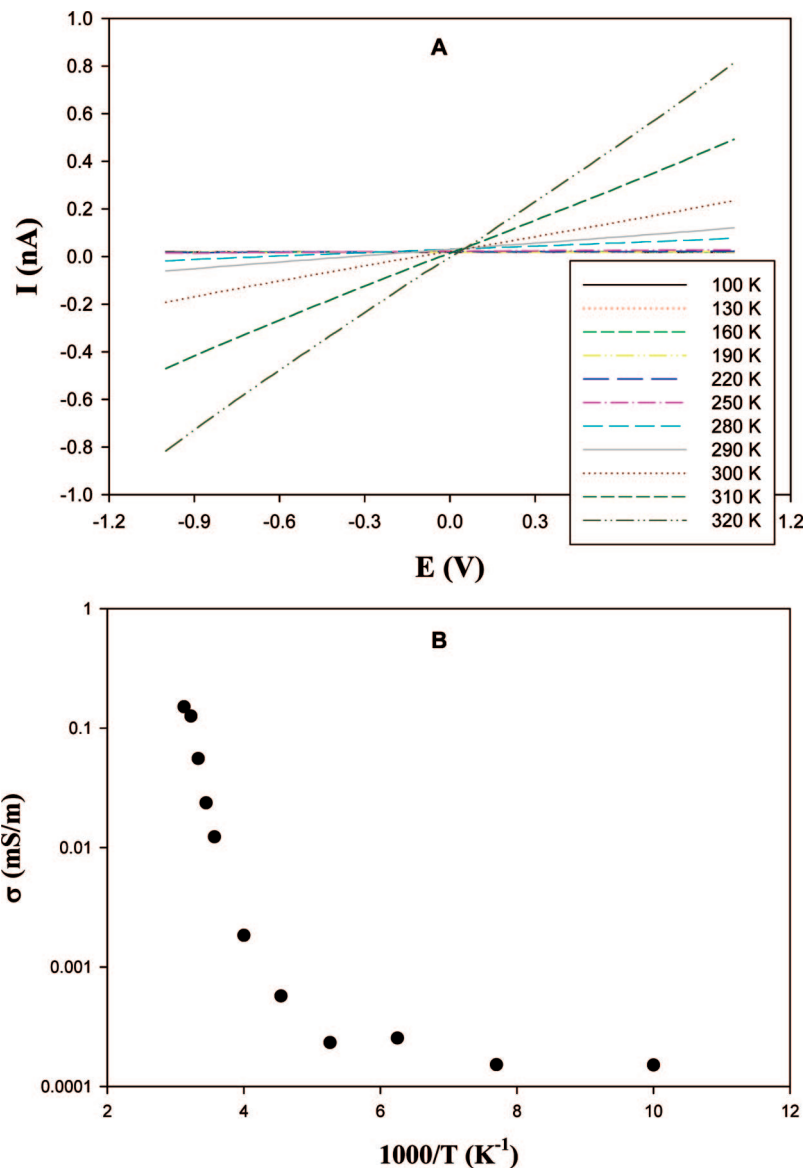
Figure 4. (A) Representative *I–V* profiles measured in the dark of a silicon nanoparticle monolayer deposited at the surface area of 109 cm^2 in the temperature range of 100–320 K. Potential scan rate 20 mV/s. (B) Variation of the particle conductivity with temperature.

presence of photoirradiation by the four different lasers. First, it can be seen that at any temperature, the higher the photon energy, the greater the enhancement of the ensemble conductivity, i.e., dark ≈ red < green < blue < UV. This can be accounted for by the increasing number of particles that are excited to generate the electron–hole pairs which are then separated by the applied electric field into free electrons, and hence enhanced photoconductivity. In fact, from Figure 2, one can see that the absorption threshold coincides with the green laser wavelength position (532 nm). Yet, this enhancement becomes less pronounced at higher temperature, because of the greater contribution of thermally activated electrons in inter-particle charge transfer, and the enhanced competition from nonradiative and radiative recombination with charge separation.[37]

Second, in the dark or with the red laser photoexcitation, the particle photoconductivity can be found to increase drastically with increasing temperature (as exemplified in Figure 4), which, as mentioned earlier, is determined mainly by the thermal activation of interparticle charge transfer. In contrast, when excited by the green, blue or UV photons, the ensemble

conductivity becomes virtually independent of temperature, suggesting that the free carrier concentration becomes saturated upon the photoirradiation by these three laser photons (although the carrier concentration increases with increasing photon energy). This implies rather efficient ionization of the photo-excited quantum-confined electron–hole pairs by the applied electric field that is aided by the relatively slow (radiative and nonradiative) recombination dynamics.[37]

It should be noted that in between laser irradiation, the ensemble conductivity was measured in the dark and the results were very consistent with those shown in Figure 4, signifying very reversible and reproducible photoconductance of the silicon nanoparticle monolayers. Also, at the end of the experiments, all particles could be removed from the IDA electrode surface by CHCl₃, and the conductivity of the electrode was virtually identical to that of the blank electrode, indicating that the particles were all chemically robust even under the repeated electrochemical perturbation and laser excitation. This is in sharp contrast to the earlier studies of the compound semiconductor nanoparticles of PbS and CdSe.[31,32]

Photoconductivity of LB Monolayers of Si Nanoparticles

J. Phys. Chem. C, Vol. 112, No. 34, 2008 **13297**
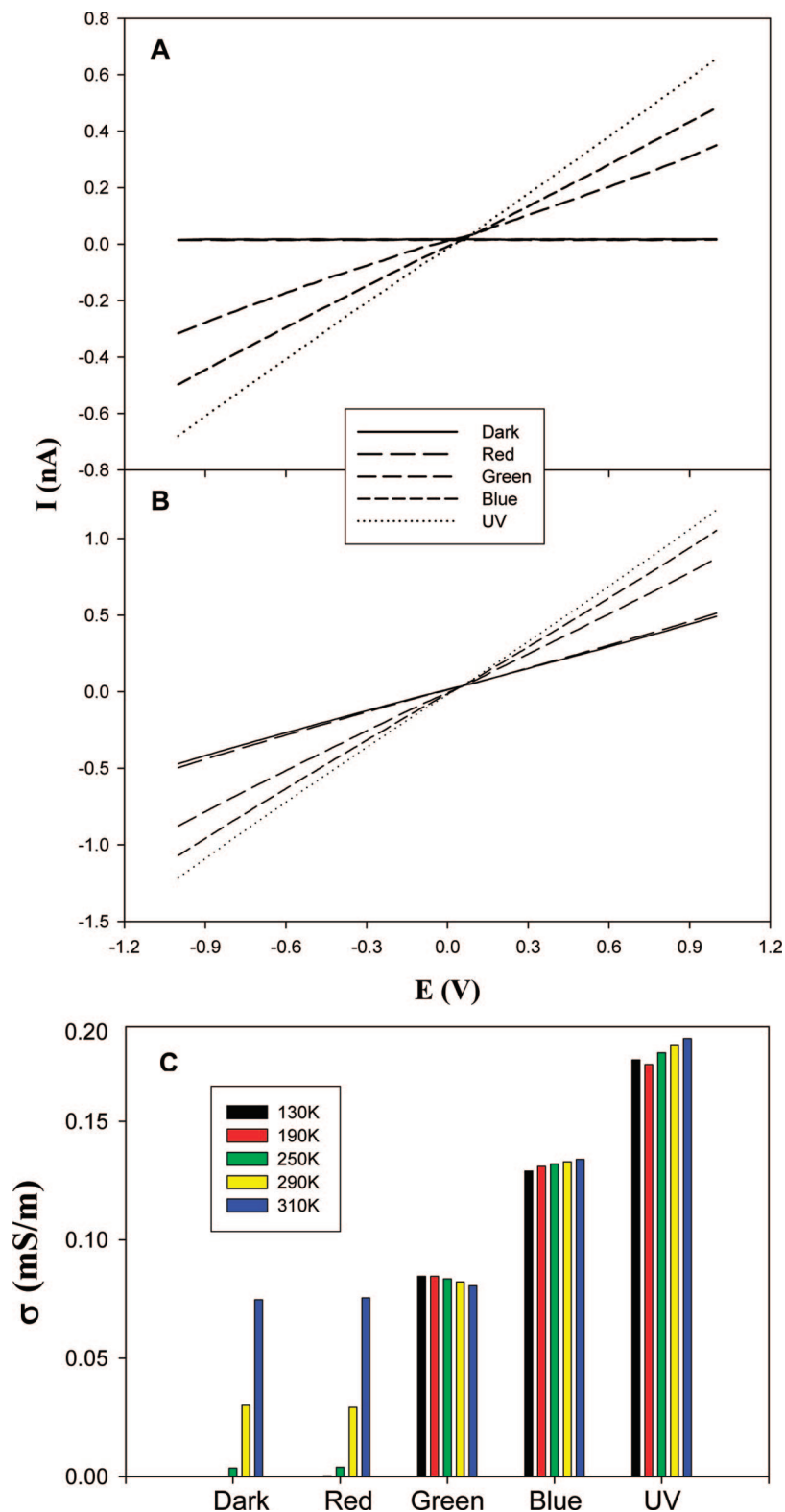
Figure 5. $I-V$ profiles of a silicon nanoparticle monolayer (same as that in Figure 4) upon the excitation by four different lasers at two different temperatures: (A) 130 and (B) 310 K. Potential scan rate 20 mV/s. Panel (C) summarizes the variation of the nanoparticle conductivity at different temperatures in the absence (dark) and presence of photoirradiation by the four different lasers.

Conclusion

The electronic conductivity of monolayers of silane-passivated silicon nanoparticles was examined in vacuum and at controlled temperature. It was observed that in the dark the particle conductivity exhibited Arrhenius-type temperature dependence at temperatures greater than 200 K, suggesting a thermal

activation mechanism for interparticle charge transfer; whereas at low temperatures (100−200 K), the conductivity was virtually independent of temperature, most likely as a result of the variable-range tunneling effect. Upon photoexcitation, the particle conductivity increased drastically with increasing photon energy; however, the enhancement effect diminished with

increasing temperature. This is attributable to the manipulation of charge carrier concentration by both thermal activation and photoinduced charge separation. Such unique characteristics might be exploited for the development of silicon nanoparticle-based photodetection in the UV to visible range, which is anticipated to have better sensitivity at lower temperature.

References and Notes

(1) Cullis, A. G.; Canham, L. T.; Calcott, P. D. J. *J. Appl. Phys.* **1997**, *82*, 909–965.

(2) Pavesi, L.; Dal Negro, L.; Mazzoleni, C.; Franzo, G.; Priolo, F. *Nature* **2000**, *408*, 440–444.

(3) Ding, Z. F.; Quinn, B. M.; Haram, S. K.; Pell, L. E.; Korgel, B. A.; Bard, A. J. *Science* **2002**, *296*, 1293–1297.

(4) Nirmal, M.; Brus, L. *Acc. Chem. Res.* **1999**, *32*, 407–414.

(5) Li, Z. F.; Swihart, M. T.; Ruckenstein, E. *Langmuir* **2004**, *20*, 1963–1971.

(6) Nakajima, A.; Futatsugi, T.; Kosemura, K.; Fukano, T.; Yokoyama, N. *Appl. Phys. Lett.* **1997**, *71*, 353–355.

(7) Schmidt, J. U.; Schmidt, B. *Mater. Sci. Eng. B* **2003**, *101*, 28–33.

(8) Ligman, R. K.; Mangolini, L.; Kortshagen, U. R.; Campbell, S. A. *Appl. Phys. Lett.* **2007**, *90*, 061116.

(9) Clemens, J. T. *Bell Labs Tech. J.* **1997**, *2*, 76–102.

(10) Paul, D. J. *Semicond. Sci. Technol.* **2004**, *19*, R75–R108.

(11) Zhao, J. P.; Meng, Y.; Huang, D. X.; Chu, W. K.; Rabalais, J. W. *J. Vac. Sci. Technol. B* **2007**, *25*, 796–800.

(12) Tsoukalas, D.; Dimitrakis, P.; Kolliopoulou, S.; Normand, P. *Mater. Sci. Eng. B* **2005**, *124*, 93–101.

(13) van Buuren, T.; Dinh, L. N.; Chase, L. L.; Siekhaus, W. J.; Terminello, L. J. *Phys. Rev. Lett.* **1998**, *80*, 3803–3806.

(14) Riabinina, D.; Durand, C.; Rosei, F.; Chaker, M. *Phys. Stat. Solidi A* **2007**, *204*, 1623–1638.

(15) Hata, K.; Yoshida, S.; Fujita, M.; Yasuda, S.; Makimura, T.; Murakami, K.; Shigekawa, H. *J. Phys. Chem. B* **2001**, *105*, 10842–10846.

(16) Mangolini, L.; Thimsen, E.; Kortshagen, U. *Nano Lett.* **2005**, *5*, 655–659.

(17) Nychyporuk, T.; Lysenko, V.; Gautier, B.; Barbier, D. *J. Appl. Phys.* **2006**, *100*, 104307–1.

(18) Aihara, S.; Ishii, R.; Fukuhara, M.; Kamata, N.; Terunuma, D.; Hirano, Y.; Saito, N.; Aramata, M.; Kashimura, S. *J. Non-Cryst. Solids* **2001**, *296*, 135–138.

(19) Nayfeh, M. H.; Rao, S.; Nayfeh, O. M.; Smith, A.; Therrien, J. *IEEE Trans. Nanotechnol.* **2005**, *4*, 660–668.

(20) Bley, R. A.; Kauzlarich, S. M. *J. Am. Chem. Soc.* **1996**, *118*, 12461–12462.

(21) Zou, J.; Baldwin, R. K.; Pettigrew, K. A.; Kauzlarich, S. M. *Nano Lett.* **2004**, *4*, 1181–1186.

(22) Zhang, X. M.; Neiner, D.; Wang, S. Z.; Louie, A. Y.; Kauzlarich, S. M. *Nanotechnology* **2007**, *18*, 095601.

(23) Wilcoxon, J. P.; Samara, G. A.; Provencio, P. N. *Phys. Rev. B* **1999**, *60*, 2704–2714.

(24) Zou, J.; Sanelle, P.; Pettigrew, K. A.; Kauzlarich, S. M. *J. Cluster Sci.* **2006**, *17*, 565–578.

(25) Zou, J.; Kauzlarich, S. M. *J. Cluster Sci.* **2008**, *19*, 341–355.

(26) Brust, M.; Walker, M.; Bethell, D.; Schiffrin, D. J.; Whyman, R. *J. Chem. Soc., Chem. Commun.* **1994**, 801–802.

(27) Templeton, A. C.; Wuelfing, M. P.; Murray, R. W. *Acc. Chem. Res.* **2000**, *33*, 27–36.

(28) Whetten, R. L.; Shafigullin, M. N.; Khoury, J. T.; Schaaff, T. G.; Vezmar, I.; Alvarez, M. M.; Wilkinson, A. *Acc. Chem. Res.* **1999**, *32*, 397–406.

(29) Therrien, J.; Belomoin, G.; Nayfeh, M. *Appl. Phys. Lett.* **2000**, *77*, 1668–1670.

(30) Ginger, D. S.; Greenham, N. C. *Synth. Met.* **2001**, *124*, 117–120.

(31) Greene, I. A.; Wu, F. X.; Zhang, J. Z.; Chen, S. W. *J. Phys. Chem. B* **2003**, *107*, 5733–5739.

(32) Pradhan, S.; Chen, S. W.; Wang, S. Z.; Zou, J.; Kauzlarich, S. M.; Louie, A. Y. *Langmuir* **2006**, *22*, 787–793.

(33) Brus, L. *J. Phys. Chem.* **1986**, *90*, 2555–2560.

(34) Sze, S. M.; Ng, K. K. *Physics of semiconductor devices*, 3rd ed.; Wiley-Interscience: Hoboken, NJ, 2007.

(35) Chen, S. W. *Anal. Chim. Acta* **2003**, *496*, 29–37.

(36) Pradhan, S.; Ghosh, D.; Xu, L. P.; Chen, S. W. *J. Am. Chem. Soc.* **2007**, *129*, 10622–10623.

(37) Leatherdale, C. A.; Kagan, C. R.; Morgan, N. Y.; Empedocles, S. A.; Kastner, M. A.; Bawendi, M. G. *Phys. Rev. B* **2000**, *62*, 2669–2680.

(38) Yu, D.; Wang, C. J.; Wehrenberg, B. L.; Guyot-Sionnest, P. *Phys. Rev. Lett.* **2004**, *92*.

(39) Pradhan, S.; Sun, J.; Deng, F. J.; Chen, S. W. *Adv. Mater.* **2006**, *18*, 3279–3283.

(40) Remacle, F.; Beverly, K. C.; Heath, J. R.; Levine, R. D. *J. Phys. Chem. B* **2003**, *107*, 13892–13901.

(41) Lide, D. R. *CRC Handbook of Chemistry and Physics; Electronic Edition*; CRC Press: Boca Raton, FL, 2001.

JP8044719